Effect of fault roughness and associated inelastic deformation on rupture propagation and seismic radiation

Report for SCEC Award 17182
Submitted June 15, 2018

PI: Eric G. Daub, University of Memphis

1 Project Overview

1.1 Abstract

This project uses dynamic rupture simulations combined with long-term tectonic modeling (LTM) to examine how heterogeneous stresses resulting from dynamic earthquake slip on rough faults influence the pattern of postseismic and interseismic strain accumulation. Off fault materials are governed by continuum plasticity in both the rupture and LTM models, while on-fault failure in the rupture model follows linear slip weakening. We examine the complex stress and damage pattern resulting from slip on a fractal fault, which creates a heterogeneous starting point from which we initiate periods of tectonic loading. We consider three separate models to compare the resulting strain accumulation, each with a different rough fault profile: one which results in supershear rupture conditions, one which results in subshear rupture conditions, and one where the rupture arrests before propagating along the entire length of the fault. We find that the heterogeneous stresses lead to localized interseismic plastic deformation, though our models show this strain accumulates in a steady manner due to the lack of time-dependent behavior in the continuum plasticity models. Future work will examine the role of time-dependent healing and velocity-dependent deformation through rate and state friction models to capture the temporal characteristics of the transition from dynamic slip to postseismic and interseismic deformation.

1.2 SCEC Annual Science Highlights

- Fault and Rupture Mechanics
- Stress and Deformation Over Time
- Dynamic Rupture Code Verification
- Computational Science

1.3 Exemplary Figure

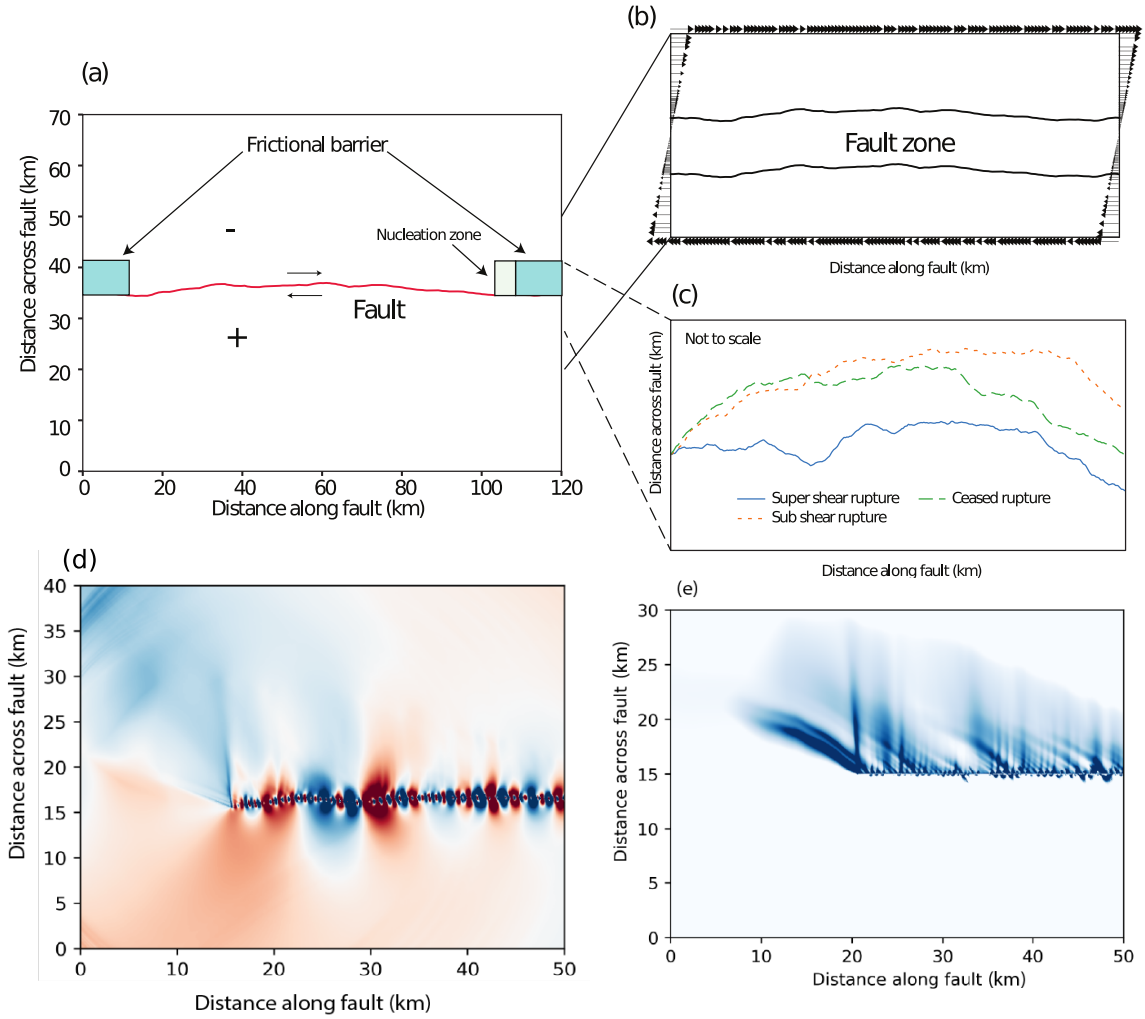

Caption: Modeling setup used to examine stress changes and postseismic deformation on a rough earthquake fault. (a) Computational domain for the dynamic rupture models. We examine spontaneous rupture on a fractal fault governed by slip weakening friction with a low dynamic coefficient of friction and allow for off-fault plastic deformation. Rupture propagation is unilateral as the nucleation zone is chosen to be at one end of the fault. (b) Computational setup for the long term tectonic (LTM) model. The rough fault with heterogeneous stress and slip is subjected to further tectonic loading to examine how continued stressing on a heterogeneous fault influences further deformation.(c) Fault profiles used in the simulation, which results in three different types of rupture: subshear, supershear, and arrested rupture. We consider multiple options to examine if there are differences in the subsequent deformation. (d) Normal stress change resulting from dynamic fault slip for the arrested rupture. The stress field prior to further tectonic loading is highly heterogeneous, ensuring that further deformation is spatially variable. (e) Plastic strain field from the dynamic rupture simulation of the arrested rupture. Damage occurs primarily on the extensional side of the fault. We find that the damaged areas are more susceptible to further deformation, indicating that they are likely to be nucleation locations of future earthquakes.

1.4 SCEC Science Priorities

3d, 2a, and 2d

1.5 Intellectual Merit

Earthquake deformation occurs over a broad range of length and time scales, and a principal goal of the SCEC collaboration is to examine these deformations using observational and computational techniques. This work introduces a new method for examining how fully dynamic fault slip on rough faults influences long-term deformation patterns on strike-slip faults. We couple the results of a spontaneous rupture model with a quasi-static long-term tectonic model, both incorporating off-fault plasticity, to examine how damage and stress heterogeneities influence the deformation patterns throughout the seismic cycle. Our research provides new tools for examining how realistic earthquake deformations observed with GPS and InSAR can be compared with numerical models.

1.6 Broader Impacts

Quantifying earthquake risk involves understanding how faults are subjected to long-term deformation and loading in order to estimate the size and location of future earthquakes. This work provides new computational methods that examine how loading and deformation processes affect faults over a wide range of length and time scales. Quantifying such processes on realistic fault geometries is essential for generating more accurate forecasts of future events. Additionally, the earthquake rupture simulation code developed in part under this award is used for education purposes through PI Daub's graduate class Earthquake Source Physics. The course involves a significant numerical modeling project using the code, where graduate students have used the code to tackle a range of simulations based on SCEC Rupture Code Verification Group.

1.7 Project Publications

Publications benefitting from this award include:

Aslam, K. S., and E. G. Daub, Effect of fault roughness on aftershock distribution: Elastic off-fault material properties, *submitted to J. Geophys. Res.*

Ahamed, S., E. G. Daub, and E. Choi, Coupling Long-Term Tectonic Loading with Short-Term Earthquake Slip and Ground Motion, *J. Geophys. Res., in revision.*

2 Technical Report

2.1 Accomplishments

This project performs numerical simulations of dynamic rupture on rough faults to quantify the stress changes and plastic deformation due to dynamic fault slip and determine the influence of this heterogeneity on interseismic and postseismic deformation. This project builds on work we have done to compare the stress change results of dynamic rupture simulations to relocated aftershock catalogs for several strike-slip earthquakes. This initial work examined the stress changes from elastic models of fault slip, and has been submitted for publication. This project extends that work to account for off-fault damage and plasticity in the dynamic rupture simulations. Previous work also examines how long term tectonic modeling (LTM) simulations can be used to set up the initial stress conditions for a dynamic rupture simulation, work that has been submitted for publication. This project builds upon those simulations by using the LTM simulations to investigate how the heterogeneous stresses resulting from our rupture simulations influence the tectonic loading and damage process over the interseismic time period. This work addresses several important science priority topics for SCEC, including developing simulations that quantify off-fault damage of earthquake slip and how stress and deformation evolve over time during the seismic cycle.

Specific accomplishments include the following:

- We perform a suite of dynamic rupture simulations on rough strike-slip faults that account for off-fault plastic deformation. Due to the varying fault roughness, ruptures exhibit a wide range of slip characteristics, including subshear rupture speeds, supershear rupture speeds, and ruptures that arrest prior to propagating along the entire fault. We save the stress and plastic strain fields at the end of these simulations, and have examined the statistical characteristics of the stress fields.

- We use the stress and plastic strain fields to initialize a new simulation using the LTM code that subjects the fault to further tectonic loading. The initial conditions reflect the heterogeneous deformation and stresses due to the earthquake. Off-fault deformation in the LTM is based on continuum plasticity, so that additional plastic deformation can occur due to the stressing imparted by tectonic loading. Our workflow allows this step to be done automatically, and thus we have the ability to examine a large suite of simulations.

- Our simulations indicate that the heterogeneous conditions from the earthquake influences the spatial locations where further deformation occurs. In particular, locations of strong extensional deformation tend to nucleate additional plastic strain, and the strong shear stress heterogeneity due to the arrested rupture crack tip also results in nucleation of further plastic deformation.

This award has resulted in conference presentations at the 2017 SCEC Annual Meeting and the 2017 AGU Fall Meeting. We have begun writing up our work for publication in a peer-reviewed journal article.

2.2 Simulation Codes

Our results make use of PI Daub's dynamic rupture code, and code development has been supported by this and other SCEC awards. Particular improvements made for this project are related to the plasticity capabilities of the code. The previous version of the code did not store the entire plastic strain tensor, as the time stepping method did not require the full strain tensor to solve the governing equations. This results in significantly reduced memory usage, but does not allow for the individual plastic strain tensor components to be output from the simulation. Instead, a scalar strain invariant could be saved to disk during the simulation. Present capabilities allow for the code to optionally store the strain tensor when individual component output is desired, but avoids storage of the full tensor in cases where that output is unnecessary.

We also use an LTM code in our work, which was developed by PI Daub's colleague Eunseo Choi. Graduate student Aslam has made a few improvements to the code for this study, in particular some changes to the options for boundary conditions to smoothly and stably impose tectonic loading (as illustrated in Fig. 1(b)). Getting our simulations to give stable results once we initialized a LTM proved to be a difficult task, but our additions to the code have resulted in a smooth transition from rupture to tectonic loading in all of our simulations. Future work will involve more significant changes to the LTM code in order to handle more complex rheologies, and Choi is a co-PI on the continuation work to oversee further code modification.

2.3 Rupture Simulations

The configuration for our rupture models is shown in Fig. 1(a). A rough strike-slip fault is subjected to a regional tectonic stress field, and we simulate unilateral rupture propagation by nucleating a rupture near one end of the fault. Examples of the fractal fault geometries are shown in Fig. 1(c). We have simulated a large number of ruptures, and choose three examples here to illustrate the various types of stress conditions and plastic strain distributions resulting from the simulations: one rupture exhibits subshear propagation, one rupture achieves a sustained supershear rupture speed, and the final rupture arrests midway through the fault due to an unfavorable bend in the fault profile.

Rupture propagation for all three fault profiles is illustrated in Fig. 2. The left set of plots show the initial shear and normal tractions resolved onto the rough fault profile. The right set of plots show normalized snapshots of the slip rate along strike of the fault at several time steps. The top plot shows the traction distribution for the subshear rupture, the middle plot shows the tractions for the supershear rupture, and the lower plot shows the tractions that result for the arrested rupture. Note that while all of the fault profiles have the same statistical properties, random variability creates different conditions that allow the ruptures to propagate differently. The subshear rupture has fairly uniform shear and normal tractions along strike, leading to steady rupture propagation (as shown in plot (b)). The supershear rupture in (c-d) exhibits lower normal tractions on the fault, allowing the shear waves radiated from the hypocenter to nucleate a second rupture that travels faster than the shear wave speed. The lower plots in (e-f) show the rupture that arrests. This particular fault profile has a patch with a high normal traction around 40 km along strike that the

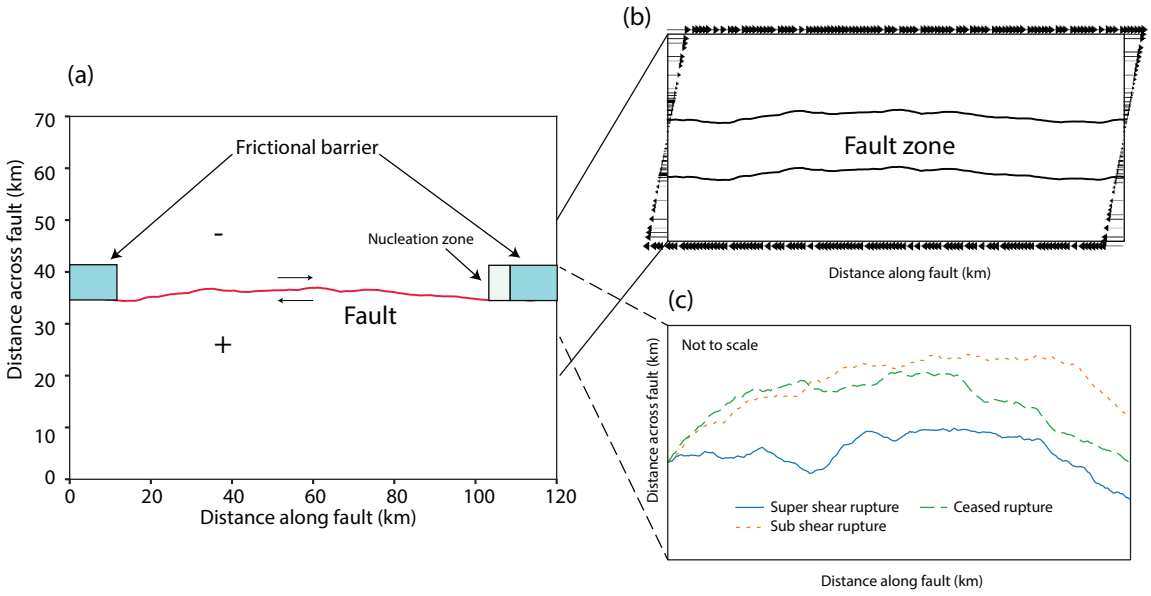

Figure 1: A sketch of the model setup for both the dynamic rupture and LTM simulation. (a) A pre-existing strike slip fault with inherent roughness is shown. The fault is 120 km long with two frictional barriers of 15 km width at each side to arrest the rupture before it reaches the edge of the simulation domain. The rupture always starts at one side of the fault so that in each case we get a unilateral rupture with plastic deformation predominantly on one side of the fault. The dominant extensional side is marked in the figure with a "−" sign while the compressional side is marked with a "+" sign. The fault roughness is characterized by a Hurst exponent $H = 1$ and a RMS roughness height of 0.01. (b) Domain setup of the LTM model. The model is driven by shear velocity boundary condition (a half plate velocity of 5 cm/yr) while the initial conditions of stress and strain are provided from the dynamic rupture model. (c) Three realization of fault profile with $H = 1$ and RMS height of 0.01. These fault profiles are used to generate three scenario ruptures: one with a supershear rupture speed, one with a subshear rupture speed, and one that arrests midway along the fault.

rupture is unable to break, leading to arrest.

The stress changes due to the three ruptures illustrated here are shown in Fig. 3. The left set of plots show the normal stress changes (negative in compression), and the right set of plots show the shear stress changes. The top figures show the stresses from the subshear rupture, the middle figures show the stress changes due to the supershear rupture, and the bottom plots illustrate the stresses from the arrested rupture. Each rupture produces a heterogeneous stress field, both in the shear and the normal stresses. We find that the exact location with the largest shear/normal stress, which is expected to be the location where further deformation occurs when tectonic loading resumes, is difficult to determine, with the exception of the arrested rupture where the majority of deformation occurs at the location where the crack tip arrested.

The plastic strain fields from the rupture simulations are shown in the plots at the left in Fig. 4. The color scale shows the second invariant of the plastic strain tensor as a function of space. Plastic deformation occurs predominantly on the extensional side of the fault.

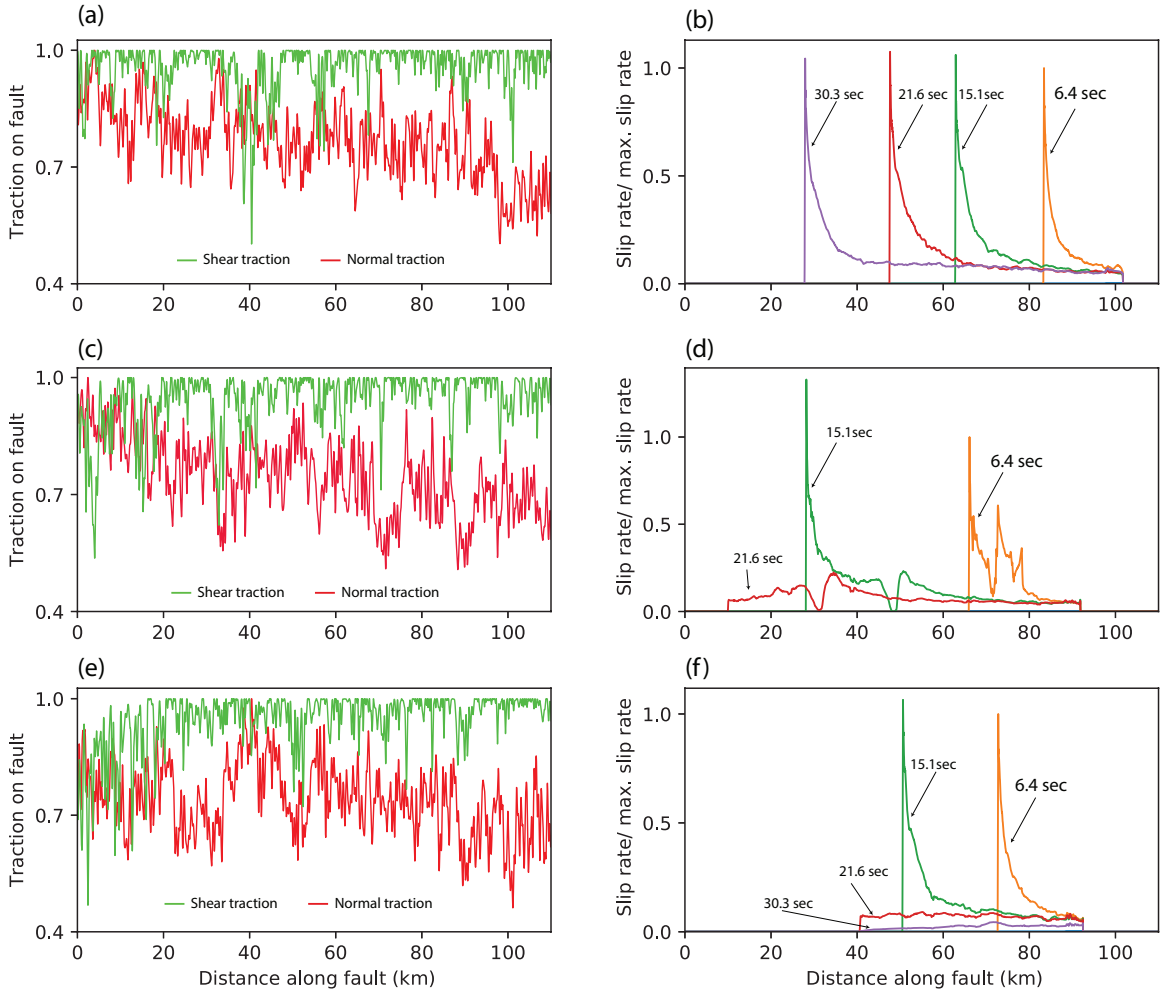

Figure 2: Plots showing initial tractions on the fault and the snapshot of slip rates along the fault at different times. Both shear and normal traction values are normalized by the maximum value. The geometry of fault profile causes the tractions on the fault to be highly heterogeneous although the regional stresses are homogeneous. The slip rate values are normalized by the maximum slip rate value at 6.4 sec. We do this to analyze if slip rate grows or decays with time as the rupture propagates. (a) Initial values of shear and normal tractions at the fault surface for the case of sub-shear rupture. (b) The slip rate along the fault at different times for the fault profile whose tractions are given in (a). The rupture initiates and continue to propagate with sub-shear velocity. (c) Initial values of shear and normal tractions on the fault surface for the case of super-shear rupture. (d) The slip rate along the fault at different times for the fault profile whose tractions are given in (c). The rupture starts with sub-shear velocity but transitions to a super-shear rupture due to favorable fault geometry. (e) Initial values of shear and normal tractions on the fault surface for the case of arrested rupture. (f) The slip rate along the fault at different times for the fault profile whose tractions are given in (e). The rupture starts as sub-shear velocity but arrests prior to propagating along the entire fault due to the fault geometry that is not favorable for further rupture propagation. Our models examine how these different scenarios influence subsequent deformation due to tectonic loading.

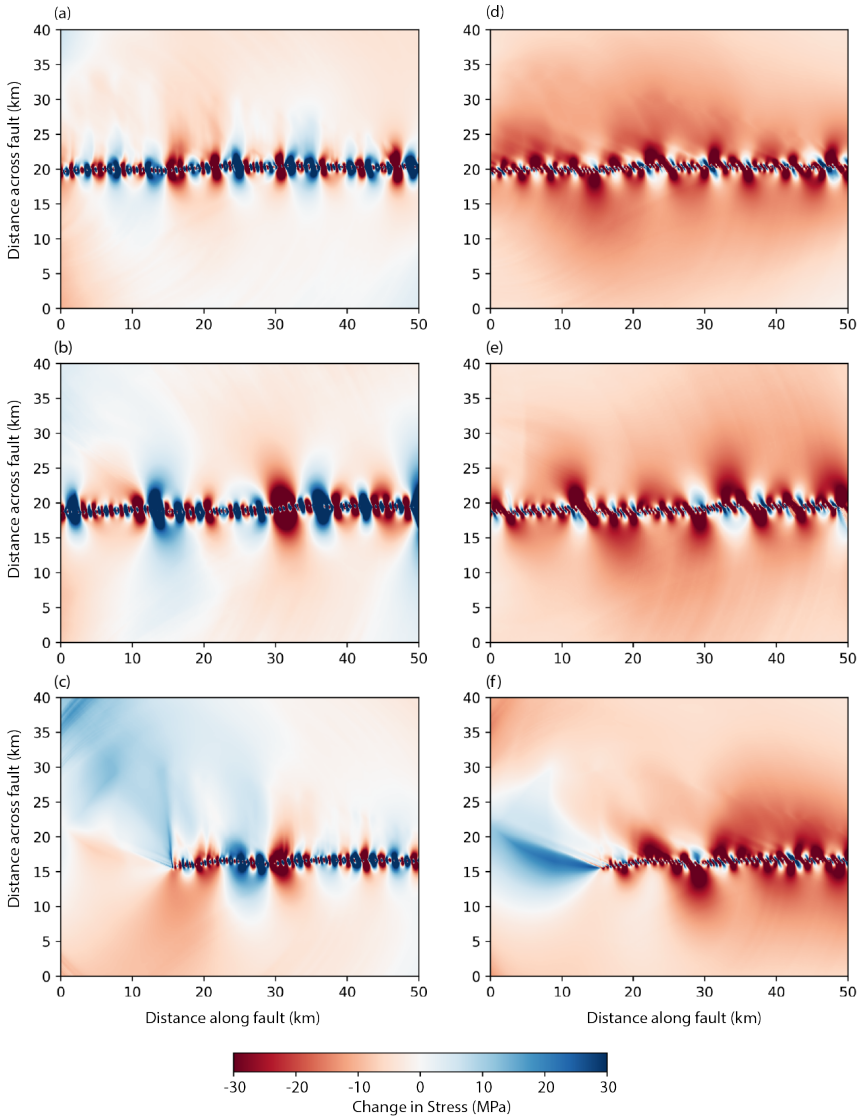

Figure 3: Change in stresses at the central part of the domain (taken from 30 to 80 km along fault and 5 to 35 km across fault distance). Figure (a), (b) and (c) are showing change in normal stresses in the central part of modeling domain (negative in compression) while (d), (e) and (f) are showing change in shear stresses in the central part of modeling domain. These stresses are taken after the rupture has propagated far enough from the central part and there are no dynamic stresses related to the wave propagation and the stress field is solely due to static stress changes. This complicated stress change will persist as further tectonic loading occurs. Left: change in normal stresses. Right: Change in shear stresses. Plots (a) and (d) are figures of sub-shear case. Plots (b) and (e) are figures of super-shear case. Plots (c) and (f) are figures where the rupture arrested. These plots illustrate that all types of ruptures produce complex stress fields, and we cannot predict which spatial locations are most likely to have conditions that will cause the following earthquake to nucleate, save for the arrested rupture where the residual crack tip stresses clearly leads to a concentration where future deformation will occur.

We note a clear difference between the plastic strain fields for the subshear and supershear ruptures: the subshear rupture exhibits patches of strong damage further from the fault than we see in the supershear rupture. The supershear rupture plastic deformation is restricted to being closer to the fault, though the differences are probably not significant enough to permit comparison with different observations of off-fault damage. This difference in spatial location is likely due to differences in the coherence of the shear waves, which carry the dynamic stresses responsible for bringing a fault to the yield point. The arrested rupture includes a strong patch of plastic strain near the crack tip that does not align with the main fault, which we will see leads to further deformation along this same direction.

2.4 Tectonic Loading on Complex Faults

Once we have run a suite of dynamic rupture simulations, we save the simulation output in order to initialize a new period of tectonic loading. This involves saving both the stress field and the plastic strain field, and using those as the initial conditions for the LTM simulation. We allow the simulation to run for a long period of time ($\sim$ 48 sec) to give the dynamic waves sufficient time to propagate away from the main part of the domain. Once these waves die away, only the static stress changes remain, which can be used as initial conditions for the quasi-static strain accumulation simulations that are common in LTM. We additionally need to save the plastic strain field, as LTM simulations often specify the cohesion to be used in the simulation by assuming cohesion weakening with plastic strain (*Lavier et al.*, 2000). This behavior is analogous to the way the friction coefficient decreases with slip according to the linear slip weakening friction law. This cohesion weakening is used to ensure that plastic strain localizes onto discrete faults in a predictable way over tectonic time scales in LTM simulations. Our use of it ensures that locations with a combination of favorable stress conditions and significant off-fault damage are susceptible to further deformation.

Results of our simulations are shown on the right side in Fig. 4. This snapshot is taken 200 years after the earthquake, and shows the results of a seismic cycle of loading added to the existing deformation field. Each rupture has nucleated several shear bands of plastic deformation. These are the locations where the next earthquake is likely to nucleate in each simulation due to the stress conditions combined with the plastic deformation leading to reduced cohesion. The arrested rupture clearly favors rupture at the arrested crack tip, though many locations in the ruptured areas of each simulation also lead to additional deformation. We find that the deformation in each case is steady with time, and does not show any particular temporal characteristics beyond the linear ramp provided by the external loading.

2.5 Future Work

Because our simulations did not show any particular temporal character, we believe that the model must capture the more complex temporal characteristics requires rheologies that are more complicated than simple continuum plasticity in order to be compared with observational data. In particular, we plan to implement a version of rate and state friction as the plasticity law, where the friction coefficient includes a rate and state dependence as observed in the laboratory. This extension will include time-dependent characteristics that have been

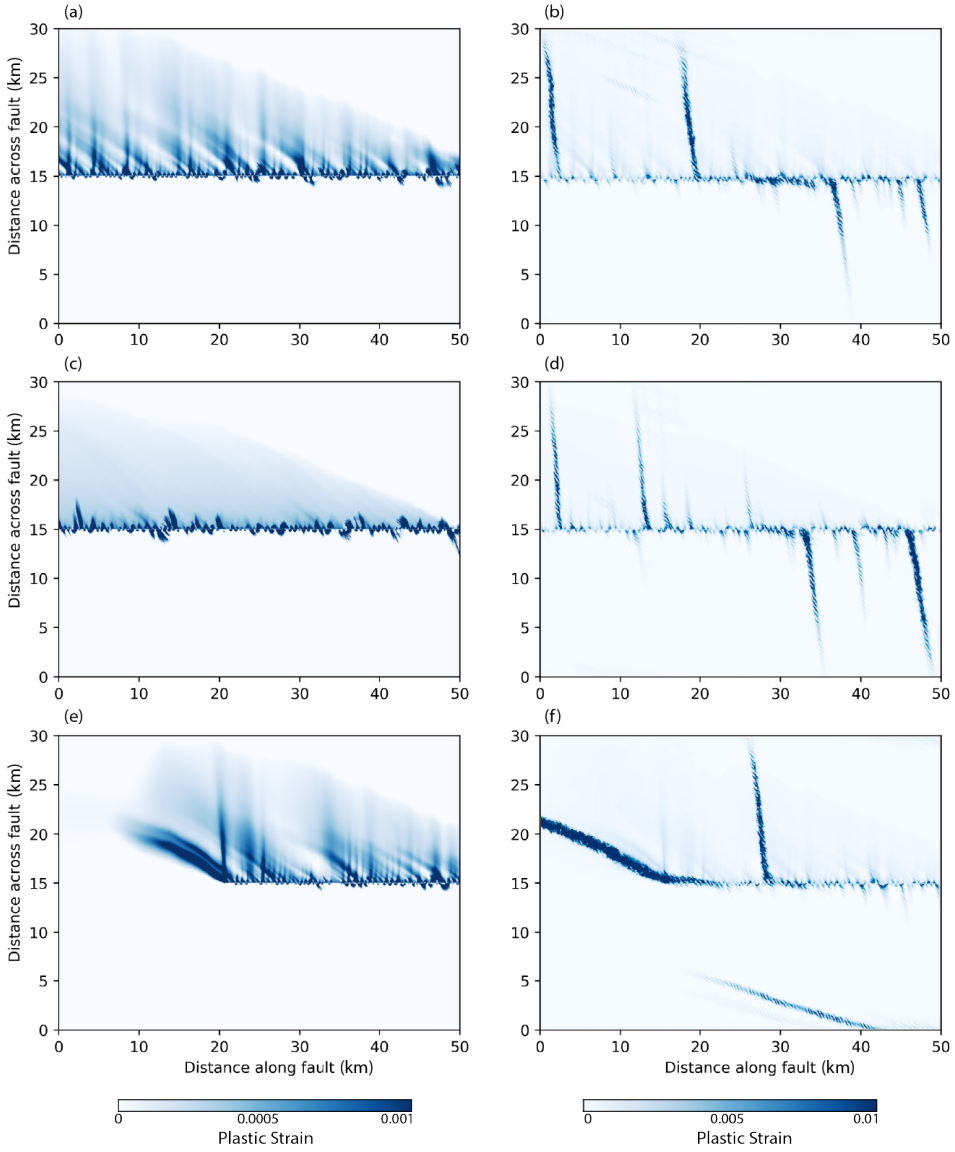

Figure 4: Accumulated plastic strain (second invariant of plastic strain tensor) at the central part of the domain. Figures (a) and (b) are for the case of subshear rupture. Figures (c) and (d) are for the case of supershear rupture. Figures (e) and (f) are for the case of arrested rupture. Figures (a), (c) and (e) are showing plastic strain accumulation at time $\sim$ 48 sec for a domain ranging from 20 to 70 km along fault distance and 15 to 45 across the fault. Figures (b), (d) and (f) are showing plastic strain accumulated after 200 years for domain 30 to 80 km along fault distance and 15 to 45 across fault distance. We have taken this sub-domain to provide results that does not involve any boundary effects. Note the different color scale for the plots on the left and the plots on the right. In each case, subsequent deformation nucleates in a spatial location where the heterogeneous stress changes lead to favorable conditions for nucleation of further deformation. This location is difficult to predict from the slip pattern, except in the case of the arrested rupture where the previous crack tip clearly leaves a stress heterogeneity that is favorable to further slip.

observed in postseismic deformation (*Barbot et al.*, 2009). In the model, time-dependent healing and velocity-dependent friction combine to lead to more complex weakening and healing behaviors. We hope that this will lead to more interesting postseismic behavior than that which we have observed in the results shown here. We plan to address this question over the next year with SCEC funds to build upon our current capabilities and create a suite of simulation tools for examining deformation processes throughout the seismic cycle on realistic earthquake faults.

2.6 References

Barbot, S., Y. Fialko, and Y. Bock (2009), Postseismic deformation due to the *mw* 6.0 2004 Parkfield earthquake: Stress-driven creep on a fault with spatially variable rate-and-state friction parameters, *Journal of Geophysical Research*, *114*, B07,405.

Lavier, L. L., W. R. Buck, and A. N. Poliakov (2000), Factors controlling normal fault offset in an ideal brittle layer, *Journal of Geophysical Research: Solid Earth (1978–2012)*, *105*(B10), 23,431–23,442.